Search for cavities in the Teotihuacan Pyramid of the Sun using cosmic muons: preliminary results.

S. AGUILAR[1], R. ALFARO[1], E. BELMONT[1], V. GRABSKI[1], T. IBARRA[1], V. LEMUS[1], L. MANZANILLA[2] A. MARTINEZ[1], A. MENCHACA-ROCHA[1], M. MORENO[1] AND A. SANDOVAL[1],

[1] *Instituto de Física, Universidad Nacional Autónoma de México, México.*
[2] *Instituto de Investigaciones Antropológicas, Universidad Nacional Autónoma de México México.*

menchaca@fisica.unam.mx, grabski@fisica.unam.mx

Abstract: Over the last two years the Pyramid of the Sun, at Teotihuacan, Mexico, has been searched for possible hidden chambers by means of muon attenuation measurements inside the monument's volume. The experimental method is based on the use of a muon tracker which is placed in a tunnel, running below the base and ending close to the symmetry axis of the pyramid. The accumulated experimental data, when compared to physics simulations using GEANT4, already show identifiable known features of the external shape of the pyramid. Experimental results of the relative density distribution inside the pyramid are presented.

Keywords: cosmic rays, muon radiography.

1 Introduction

Among the increasing number of applications for atmo spheric muon attenuation to investigate the internal struc tures in large volumes, its use to tackle archaeological problems stands out as one generating special public inter est. Following the classical experiment by Alvarez et al. [1] who searched for cavities in Chephren, one of the famous Egyptian pyramids, over the last decade we setup and ran an experiment applying a similar technique to investigate the Mexican Pyramid of the Sun at Teotihuacan, hereafter referred to as Pyramid of the Sun. The project, and its first results, have been reported before in this conference series [2, 3]. Here we present a progress report, after two years of data taking, which includes comparisons with GEANT4 [4] Monte Carlo simulations to reveal emerging interesting aspects of the data.

2 Experimental setup

The external topology of this monument, extracted from a level diagram obtained using a aero-photographic tech nique, is shown in Fig. 1. Beyond the overall pentahe dral shape, when compared to the Egyptian pyramids, the Teotihuacan monument shows important topological differ ences. Some of them are:
(a) a flatter aspect ratio (half the height and a similar size square base as Chephren);
(b) a 5-level external corridor structure, irregularly dis tributed in height;
(c) a well defined front-face, having an extra pyramid body in its lower part, as well as (less pronounced) external climbing-stairs;
(d) a system of man-made tunnels dating from different stages of the monument's existence.
Our detector is installed in a 4-leafed clover-shaped cave, located some 34 m west (and 10 m south) of the (verti cal) symmetry axis of the pyramid, at the end of the sole pre Hispanic (believed to be pre-pyramid) tunnel, which runs 8 m below the pyramid. A second tunnel, roughly one century-old, runs centered across the pyramid (front-

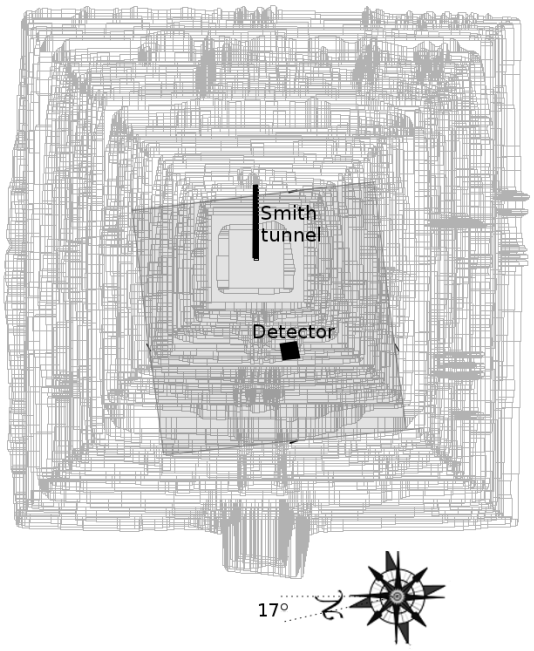

Fig. 1: External shape of the Pyramid of the Sun. Detector approximate field of view, projected on the monument's surface, is highlighted

to-back), along the first level (counting from the bottom of the pyramid, up). One last tunnel (called Smith, after its creator), excavated 50 years ago, runs from the back to the core of the monument, ending near its (vertical) symmetry axis, along the 5th body (i.e., one before the top). Because of the $\approx 35m$ displacement from the symmetry axis, only the Smith tunnel lies within the field of view of our detector, in its vertical orientation.
Thus, besides the pyramid's top itself, the more noticeable external structures within the detector's observation solid angle are the upper-most 4 corridors The detector array

consists of four 1m x 1m scintillators used to generate the muon trigger, and six MWPC's (also having 1m x 1m sensitive area) for muon-tracking purposes. Basic details about the experimental setup may be found in[3]. The sintillator counters are arranged by pairs to form two planes, separated 75 cm. To enlarge the trigger solid angle, these planes are located as follows: one at the bottom of the detection system, and one below the top-most two MWPC's. The scintillators in each plane are operated in a logic OR mode. This way, the individual scintillator efficiencies, ranging between 70% and 90%, result in a 94%-97% efficiency for each plane. A logic AND between the two scintillator planes constitute the trigger, yielding a mean 92% efficiency. The efficiency of each MWPC is measured using the trigger. This method requires a geometrical correction for the two top-most MWPC's.The resulting full 3-point track reconstruction efficiency turned out to be below 10%. Data taking has also been impacted by external factors, such as data-network connectivity and electric-power failures, as well as MWPC gas-mix quality fluctuations, which at times introduced up to a further 50% efficiency reduction. A contribution from accidentals of approximate 20 % has been estimated using the time-of-flight (TOF) spectrum between two scintillator planes within a 80ns time window. So the estimated count rate is about 2.7 $\pm$0.05 Hz, which is close to the Monte-Carlo simulation predictions of 2.62, reflecting that the detector position, pyramid average-thickness and average density used in the simulations are consistent with the observation. The muon-track coordinate corresponding to each chamber has been estimated by means of a Flash ADC (FADC) signal shape analysis technique[5]. The tracks have been reconstructed using information from three chambers for each coordinate. More details about the track reconstruction, coordinate and angular resolutions can be found in [3].

3 Signal processing and DAQ

Standard NIM electronics modules are used to process the scintillator and MWPC signals. The preamplified analogic signals from the two extremes of each MWPC were digitized using CAEN v1729-VME 4- channel 12 bit sampling-FADC. More details about DAQ system can be found in [3]. The digitized data processing has been carried out using a single board CPU Concurrent Technology [6]. The read-out is synchronized with the trigger interruption. The trigger time is fixed using CPU Unix time, which is recorded for each trigger. An overall busy signal is generated using a logic OR between the hardware and software busy signals, and have been used to veto the trigger coincidence module. The read-out dead time turns out to be of order of 10ms, not representing a problem for our Hz-range trigger rate. The generated weekly volume of data information is about 100Gb.

4 MC-simulation

Muon transport through the detector, as well as through the body of pyramid, has been simulated using the GEANT4 Monte Carlo package [4]. This allowed us to estimate both, the detector geometrical efficiencies, as well as the expected muon-flux distribution inside the pyramids cave, where the detector is located. For this purpose, the assumed pyramid material composition as well as its external shape,

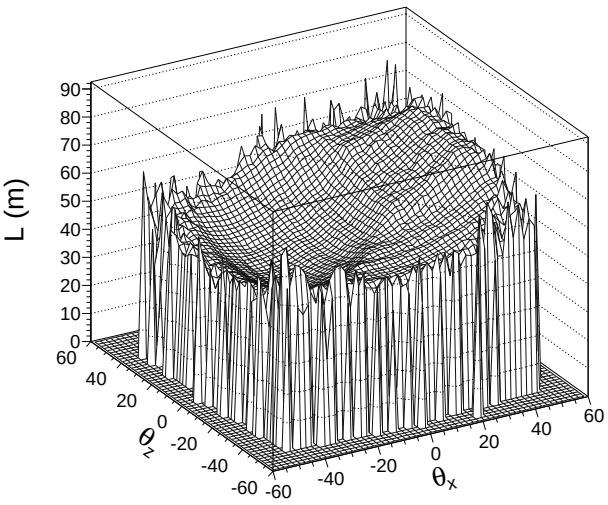

Fig. 2: Angular distribution of the pyramid thickness in detector acceptance. The distribution is obtained from the pyramid digitized data, see the text.

as described in Section 2 have been introduced to the M-C code. More details about the pyramid geometry construction, precision, and detector position may be found in [3, 7]. The simulation indicates that only muons having $\geq 200MeV$ kinetic energies can cross the detector's volume. Above that threshold, the detector geometrical efficiency has been estimated assuming a (muon) power-law spectrum. The average mater thicknesses distribution of the pyramid for different (detection) projection-angles is presented in Fig 2. There we see that the observed pyramid thicknesses vary between 40 to 80m, with a minimum located around the angles $\theta_x = -29, \theta_z = 4$). Figure 2 represents the pyramid's material distribution, as sampled by the muonic flux incident on the detector, averaged along the simulated particle tracks, i.e., including multiple scattering effects. Although the off-symmetry location of the detector complicates the identification of its structures with those shown in Fig. 1, certain features can be easily recognized. For example, a straight ridge approximately directed towards the (-60,-60) corner of Fig. 2 corresponds to the nearest (south-west) edge of the pyramid. Crossing it near $\theta_z = 0$ degrees, and running perpendicularly towards the high θ_z region, is the ridge corresponding to the north-west edge of the pyramid. Of the other two pyramid edges, only their top ends are encompassed by the detector observation solid angle, so they are more difficult to identify in this figure. Having its minimum located (nearly) symmetrically along the $\theta_z = 0$ axis, but off towards the negative side of the θ_x axis, the distribution shown in Fig. 2 clearly reflects the detector location, having (within its observation solid angle) more pyramid matter on the positive θ_x side than on the negative-value side. A sharp-eye may identify the small square base at the top of the pyramid, and even traces of the Smith tunnel. At this level of detail, one may also remark small structures at the Fig. 2 valley (running parallel to the θ_z axis), which correspond to the front-face level-structure of the pyramid. The simulation prediction for the muon rates, corrected by the detector geometrical efficiency and dependent on the projection angles at the detector location, is shown in Fig 3. As expected, the topology of this distribution is anti-correlated with the pyramid thick-

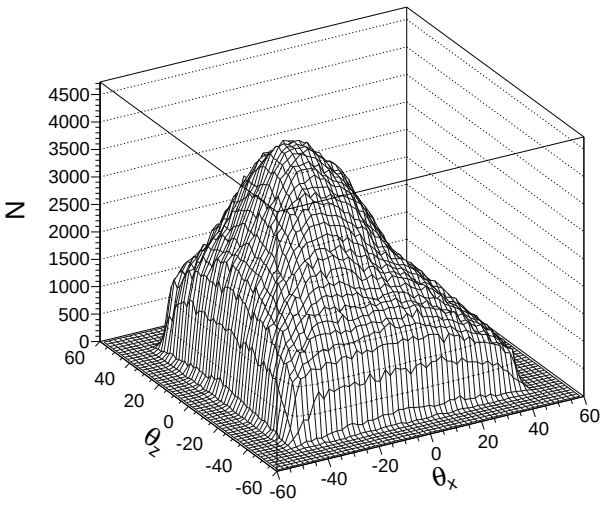

Fig. 3: Angular distribution of simulated events corrected by the detector acceptance in the detector cave. The distribution is normalized to the one in in Fig. 5.

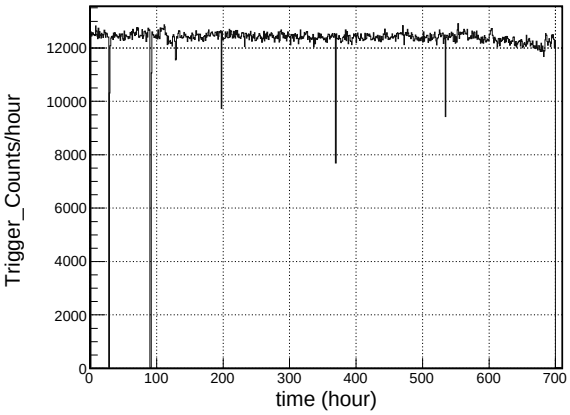

Fig. 4: Trigger count rate for a one-month time period. The vertical lines in the plot are due to the interruptions in data collection time.

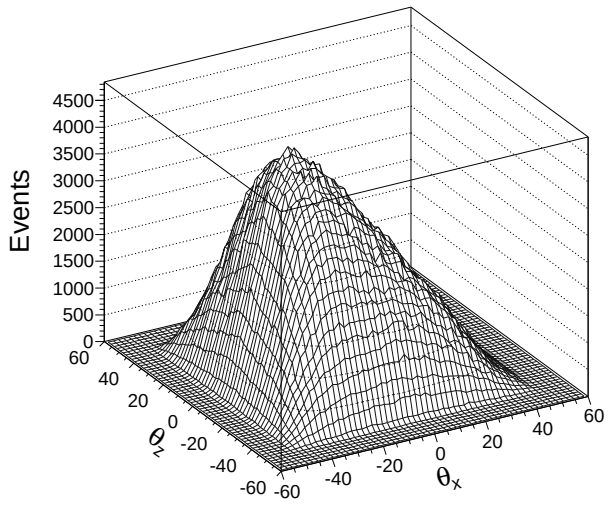

Fig. 5: Angular distribution of detected events, see the text.

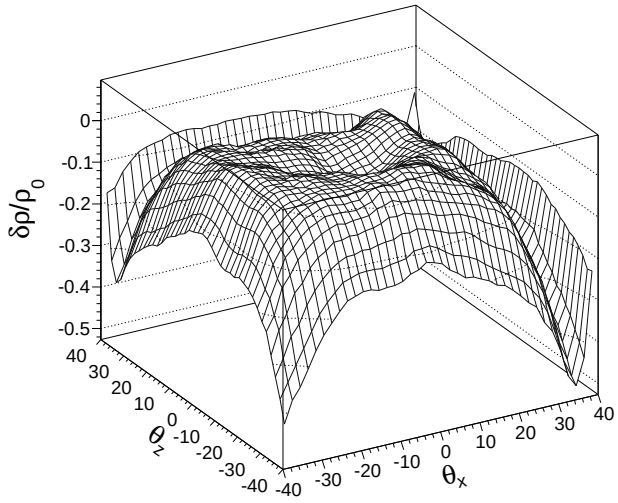

Fig. 6: Preliminary data of relative density distribution inside the pyramid volume.

nesses distribution shown in Fig 2. This is because less thickness results on a higher muon count-rate, and vice-versa. Thus, the maximum in Fig. 3 (off-centered towards negative θ_x values, but nearly symmetric relative to the θ_z axis, corresponds to the Fig. 2 valley. Detector acceptance deforms (sharpens) the Fig. 3 distribution, making more difficult a direct pyramid-structure identifications. In particular, note that the high θ_x region, where the Smith tunnel is located, lies in the low count-rate region.

5 Experimental Results

Before presenting our two-year result, the reader should be aware that, because of practical reasons (no adequate accelerator facility in the Country), the present experiment lacks of energy-, and position-, dependent efficiency measurements for the individual, and/or the integrated detection system. Still, the fact that the scintillator-counting system has remained very stable during the experiment (see Fig. 4) allows us to contemplate approximate means to evaluate our position-dependent efficiency from track correlations. The preliminary two-dimensional projection-angle plot of the number of detected events is presented in Fig 5 (already corrected by non uniform chambers' surface response), to be compared with Fig 3. There is an overall similarity between the two figures, including the multiply mentioned θ_z nearly symmetry and θ_x asymmetry. However, on a closer look one can notice slight differences, such as the position of the maximum along the θ_x axes. Using the experimental and MC (normalized to experimental) distributions of muon rates, the relative density distribution inside the pyramid can be estimated using the power-law behavior of the muon flux [8] as shown in Fig. 6. Here one can notice that the most appreciable differences are observed in the large-angle regions, what can be the result of two types of errors: the difference between the assumed pyramid external geometry in the simulation, compared with the real one, as well as errors in the detector efficiency estimation.

No immediate comparison can be made between the pyramids external shape (Fig. 1) and the thickness distribution of Fig. 2, because they represent different perspectives, one corresponding to an outside viewer, located high above, and along the vertical symmetry axis of the monu-

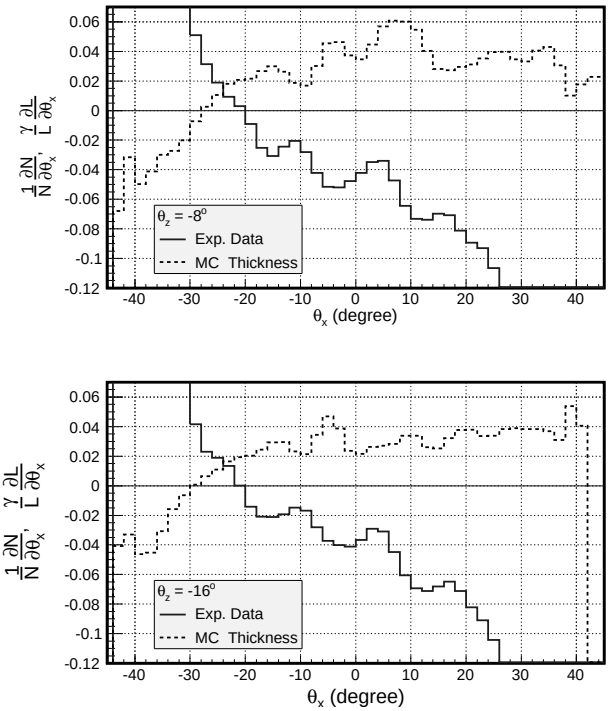

Fig. 7: Estimated derivatives from the Fig 2 and Fig 5 for two different intervals of projection angles θ_z dependent on the projection-angle θ_x, are drawn. For line interpretation see inset.

ment, while the second represents the vision of an observer looking from below, through a square-section cone, located 35 m far from the same symmetry axis. Image recognition is further complicated by the detectors geometrical efficiency, making it harder to recognize some features in, either the simulation (Fig. 3) or the data (Fig. 5). Still, the geometrical information is there, and can be enhanced using angle derivatives. This way, the relation between the muon count $N(L,\theta_x,\theta_z)$ and the average pyramid thickness $L(\theta_x,\theta_z)$ for a given angular bin, neglecting angular dependence of the muon flux, can be written as [8]:

$$N(L,\theta_x,\theta_z) \approx CL(\theta_x,\theta_z)^{-\gamma} \quad (1)$$

Here C is the normalization constant and we are using a $\gamma \approx 1.81$ constant approximation [7]. In this case, the partial derivatives respect to θ_x for a fixed θ_z can be written as:

$$\frac{1}{N}\frac{\partial N}{\partial \theta_x} \approx -\frac{\gamma}{L}\frac{\partial L}{\partial \theta_x} \quad (2)$$

Then, the event distribution is significantly modified by the detector efficiency(the contribution of flux angular dependence is less than 20% for the energies $> 20GeV$ and for zenith angles < 40 degree [7]) and one should expect similar mirror (anticorrelated) structures respect to zero. In Fig 7 these derivatives for two different θ_z windows with average values $-16(-20,-12)$ and $-8(-12,-4)$ are shown. The choice of θ_z values is to minimize the contribution of the detector efficiency, increasing the statistics. As can be seen from the figure in the θ_x angular region -20 to 20 we observe clear anticorrelated, structures. These correlations have been used to tune the detector position in simulation geometry.

6 Conclusions

Progress in the muon attenuation experiment carried out at the Pyramid of the Sun, in Teotihuacan, Mexico, is reported, including experimental and simulation details. The gross structural differences obtained while comparing data and simulations may reflect uncertainties resulting from a limited knowledge of the pyramid external shape, internal density distribution, as well as the lack of space-energy detection efficiency measurements. In spite of that, which is coupled with large efficiency problems, after two years-worth of data, the experiment-simulation comparisons show encouraging qualitative and quantitative resemblances. We are working to obtain independent detector efficiency estimates, which included in the final results, shall be presented in a later publication.

Acknowledgment: Authors acknowledge the partial support from CONACYT grants G39091-E and 131877 as well as PAPIIT-UNAM grants IN115107,IN111612.

References

[1] L.W. Alvarez et al., Science 167, (1970) 832.
[2] R. Alfaro et al., Proceedings of the 30th ICRC, Vol. 5 (HE part 2), pages 1265-1268.
[3] S. Aguilar et al., Proceedings of the 32th ICRC, Vol. 4, p 317
[4] S. Agostinelli et al., Geant4 a simulation toolkit, Nucl. Instr. Meth., A506, (3), 2003, P. 250-303
[5] M. Lopez-Robles et. al. IEEE Tr. Nucl. Sc. 52 (2005) 2841-2845.
[6] http://www.cct.co.uk/
[7] V. Grabski et al, NIM A 585 (2008) 128-135.
[8] Malmqvist, et al, 1979, Geophysics, 44, 1549-1569.